Peer review status: This is a non-peer-reviewed preprint submitted to EarthArXiv

This manuscript has been submitted to the Journal of Structural Geology for peer review in June 2026.

Inferring the sub-surface connectivity and structural maturity of the Roccapreturo normal fault system, Central Apeninnes, Italy, using high-resolution structural mapping

Zoë K. Mildon[1], Billy J. Andrews[1,2], Francesco Iezzi[3], Marco Mercuri[4], Joanna P. Faure Walker[5], Gerald P. Roberts[6], Constanza Rodriguez Piceda[1,7]

1. School of Geography, Earth and Environmental Sciences, University of Plymouth, Drake Circus, Plymouth, UK (corresponding author, zoe.mildon@plymouth.ac.uk)
2. Department of Earth Sciences, Durham University, Durham, UK
3. Department of Earth Sciences, Environment and Resources, University of Naples Federico II, Naples, Italy
4. Dipartimento di Scienze della Terra, Sapienza Università di Roma, Roma, Italy
5. Department of Risk and Disaster Reduction, University College London, London, UK
6. School of Natural Sciences, Birkbeck, University of London, London, UK
7. Dipartimento di Scienze, Università degli studi Roma Tre, Roma, Italy

Abstract (250 words)

Constraining how active faults link together in the sub-surface and understanding how fault geometry and structural maturity affect earthquake propagation are key tools for understanding earthquake behaviour and seismic hazard. We use the Roccapreturo fault system, from the Central Apennines, Italy, which has three closely spaced normal faults mapped at the surface as a case study to explore these questions. Here we present a high-spatial-resolution database of structural (strike/dip) and kinematic (trend/plunge of slip vectors) measurements, as well as Holocene and geological throw measurements. We find that the fault geometry is highly variable, with strike ranging from 072° – 183°, dip varying from 42 – 82°, and the fault trace is variably segmented along-strike. Steeper fault dips occur within a relay zone between two strands. We interpret this observation as supporting evidence that these fault strands are connected in the sub-surface. Twelve Holocene throw profiles and seven geological cross-sections were collected, the maximum Holocene throw is

8.75 ± 1.75 m (giving a Holocene-averaged throw rate of 0.58 ± 0.16 mm/yr) and the maximum geological throw is 610 m (giving a T/L ratio of 0.055). Strain rate calculations, using the high-resolution structural, kinematic and Holocene throw data, show a smooth variation in the strain rate of the fault, despite complex surface geometry, implying that the fault geometry and slip are coupled. Our results demonstrate the value of high-resolution fault mapping where possible, to discern the maturity, sub-surface linkage and therefore potential earthquake rupture dynamics of active faults.

Introduction

When considering earthquake occurrence, fault interaction and resulting seismic hazard, it is important to characterize the geometry of active faults and fault systems (i.e. segmentation, changes in strike and/or dip), including how the geometry of the fault(s) change with depth. This is because these factors affect the estimation of maximum earthquake magnitude and coseismic slip when scaling laws are used (Manighetti et al., 2007; Stirling et al., 2013; Thingbaijam et al., 2017; Wells & Coppersmith, 1994). Commonly, faults grow by tip growth and linkage to adjacent pre-existing faults, generating relay zones and fault bends in the process (Cartwright et al., 1995; Mansfield & Cartwright, 2001; McLeod et al., 2000) (Figure 1b). There are times during the process of fault linkage when the 3D structure of a fault is complex, for example when a single fault at depth may appear as two (or more) separate faults at the surface (e.g. Figure 1b, Time 5) (Giba et al., 2012; Roche et al., 2021; Walsh et al., 2003). This highlights the importance of being able to characterise both the surface and sub-surface geometry of active faults.

Knowing whether presently active faults connect or not in the sub-surface is important for understanding and quantifying seismic hazard, yet this may be challenging to constrain. Understanding fault connectivity at depth is important because fault scaling laws are commonly used to calculate the expected earthquake magnitude and maximum coseismic slip for seismic hazard assessment from the fault length (Manighetti et al., 2007; Stirling et al., 2013; Thingbaijam et al., 2017; Wells & Coppersmith, 1994). Fault bends and fault segmentation may control the extent and propagation of earthquake ruptures (e.g., DePolo et al., 1991; King & Nabelek, 1985; Mildon et al., 2019; Pizzi et al., 2017). Furthermore, it has been suggested that the structural maturity of a fault may control the dynamics of earthquakes (Perrin et al., 2016). Structural maturity is challenging to define quantitatively

(see (Manighetti et al., 2021) and references therein), but overall as a fault becomes more mature by accumulating slip, the stress drop of large earthquakes is hypothesised to be lower (Choy & Kirby, 2004; Hecker et al., 2010; Manighetti et al., 2007). Additionally, if faults are more immature, then studies suggest that there will be more stress heterogeneities (Hayek et al., 2024), more distributed damage (Thakur & Huang, 2021), more aftershocks (Guo et al., 2023), irregular recurrence intervals (Thakur & Huang, 2021) and less efficient rupture propagation of earthquakes (Andrews et al., 2026; Guo et al., 2023). Therefore, understanding the connectivity and structural maturity of faults is useful to understand potential earthquake behaviour, especially if the fault of interest has not ruptured in historical or instrumental times.

Where it is not possible to measure fault connectivity directly, e.g. by using 3D seismic reflection data, it is often possible to infer linkage using surface observations. Normal faults can be hypothesised to connect in the sub-surface based on the occurrence of convergent slip vectors (Faure Walker et al., 2010; Roberts, 2007; Roberts & Michetti, 2004). Geomorphology can be used to speculate on sub-surface fault connectivity, if there is a continuous footwall-uplifted mountain range and/or a continuous down-throw hangingwall basin, this would imply that there is a continuous fault controlling the uplift/subsidence.

Another approach to elucidate fault connections in the sub-surface is to utilise the so-called geometry-dependent throw-rate model (Faure Walker et al., 2009, 2015, 2019) (Figure 1c). This model theorises that, to maintain the strain rate across a fault when there is a change in strike in the fault trace, the dip and throw of the fault must co-vary. In particular, the model predicts that when there is an along-strike bend in the fault, the fault should steepen (i.e. the dip increases) and the throw should also increase. This model has been demonstrated to hold for both coseismic (Iezzi et al., 2018; Mildon et al., 2016) and Holocene (Faure Walker et al., 2009; Sgambato et al., 2020; Wilkinson et al., 2015) throw on normal faults in the Apennines. However, none of these studies have explored whether this model applies to linkage zones where fault bends may exist at depth but not yet propagated to the surface. To use the geometry-dependent throw-rate model to infer sub-surface fault linkage, high resolution geological mapping of surface fault scarps is essential to constrain the location, geometry and slip rate of faults. We propose that this field data can be used to identify areas

of a fault or fault system with higher-than-expected dips and throws, which may indicate that faults are connected in the sub-surface.

The ~10 km long Roccapreturo fault system is located in the extensional region of the Central Apennines, Italy. There is a well-preserved bedrock scarp along much of the fault trace, making this an ideal case study to a) gather high resolution structural data and b) use this to speculate on sub-surface connectivity and rupture dynamics of an en-echelon fault system Previous studies have suggested that the Roccapreturo fault strands link in the sub-surface to form a single structure (Iezzi et al., 2025; Roberts et al., 2025), including the "Main Fault" level in the Fault2SHA database (Figure 1a) (Faure Walker et al., 2021). This suggestion is based on the proximity of the faults which are separated by 0.5 – 1.5 km at the surface and the presence of convergent slip vectors along the length of the fault. Additional constraints on the sub-surface geometry would strengthen this hypothesis. However, there are open questions about how the splays interact together and how the maturity of the fault may affect earthquake behaviour. This study presents a high spatial resolution structural database of the geometry, kinematics and throw (both Holocene and geological) along this fault system, and we used this data to calculate the along-strike strain distribution. Our work allows us to verify whether these fault strands are connected at depth, and to elucidate the variations in geometry and strain rate along the fault system. The sub-surface connectivity and complex surface fault trace may have implications for the magnitude, occurrence and propagation of future earthquakes across this fault system.

Geological background

The Central Italian Apennines are a region of active NE-SW extension, accommodated by a series of predominantly NW-SE striking normal faults (Figure 1a). The region is extending at a rate of 2.7 ± 0.2 mm/yr based on GNSS data (D'Agostino et al., 2011), which agrees with the Holocene extension rate of 3.1 ± 0.7 mm/yr from measuring bedrock fault scarps across the region (Faure Walker et al., 2010). Extension began ~2-3 Ma and was preceded by a phase of compression from the Miocene to early Pliocene due to subduction that has since undergone roll back to the north-east (Anderson & Jackson, 1987; Carminati et al., 2012; Cavinato & De Celles, 1999; Piccardi et al., 1999). Carbonate bedrock fault scarps are well

exposed throughout the region, these scarps have formed since the demise of the Last Glacial Maximum when erosion rates reduced, hillsides stabilised and offsets generated by earthquakes could be preserved and accumulated (Piccardi et al., 1999; Roberts & Michetti, 2004; Tucker et al., 2011). The age of the end of the Last Glacial Maximum is taken to be 15 ± 3 kyrs, based on cosmogenic dating of hillsides (Cowie et al., 2017), changes in pollen from lake cores (Allen et al., 1999) and dating glacial features (Giraudi & Frezzotti, 1997).

The Roccapreturo fault system forms part of the Middle Aterno Valley fault system (Faure Walker et al., 2021; Galadini & Galli, 2000), as defined at the "Main Fault" level in the Fault2SHA database. The Fault2SHA database is compilation of published field data for active faults in the Central Apennines, including fault locations, geometry, slip rates, and activity levels, and it aims to be a conceptual framework to gather and present fault data used for seismic hazard assessment (Faure Walker et al., 2021). The database has three levels, "Traces", "Faults" and "Main faults". "Traces" are the primary level of data and are defined by constant location certainty (i.e. how well constrained is the fault trace) and activity scale (i.e. level of certainty that the fault was active in the Holocene or Pleistocene) along the length of the trace. "Faults" are how Traces are connected together at the surface and/or at depth, and are based on the continuity of fault geometry, Holocene/geological offsets or known earthquake ruptures. "Main Faults" represent how Faults are interpreted to be linked at depth and is the recommended level for seismic hazard models. Following the Fault2SHA database at the "Fault" level (Faure Walker et al., 2021), three strands to the Roccapreturo fault system are identified – the Roccapreturo, Middle Aterno Valley West and Succiano faults (Figure 2a). The three strands are closely spaced together, with a separation of 0.5 – 1.5 km between the strands, and the along-strike overlap between the strands is ~3.5 km. Note that the Fontecchio fault also forms the Middle Aterno Valley Main Fault, but we omit this from our study because 1) the Fontecchio fault is poorly exposed in the field, and 2) we focus on the three overlapping fault splays to explore their interaction and linkage. At the "Trace" level in the database, the three faults are made up of several traces: the Middle Aterno Valley West Fault comprises the Santa Maria Del Ponte West, Tione Degli Abruzzi West and Tione Degli Abruzzi East Traces, the Succiano Fault comprises the Succiano San Lorenzo and Beffi Traces, the Roccapreturo Fault comprises the Roccapreturo North West, Roccapreturo Acciano and Acciano Traces (Figure 2a).

The presence of a well-developed bedrock fault scarp, particularly along the Roccapreturo segment, indicates that this fault has been active during the Holocene (Figure 3). The fault scarps associated with the Middle Aterno Valley West and Succiano Faults are less continuous, but the oversteepening associated with a fault scarp and geomorphology are broadly continuous along these faults, also suggesting that these faults have been active during the Holocene. Paleoseismic and cosmogenic studies have been conducted along the Roccapreturo Fault to determine the recent slip history. A paleoseismic study (Falcucci et al., 2015) found two surface-faulting earthquakes in the last 5,000 years, with the most recent occurring between 1,879–2,009 BP and 3,787–6,055 BP. Accumulation of cosmogenic nuclides up the fault scarp have been used to investigate the slip history of the fault over the Holocene (Roberts et al., 2025), which suggests a rapid slip rate (i.e. earthquake clustering) over the last 1.5 kyrs. However, there are no historically recorded earthquakes associated with this fault (i.e. >700 years since the most recent event, (Galadini & Galli, 2000; Guidoboni et al., 2019)), therefore the elapsed time on this fault is at least 700 years. The nearest large recent earthquake was the Mw 6.3 2009 L'Aquila earthquake (Alessio et al., 2010; Walters et al., 2009), which ruptured the Paganica San Demetrio Ne Vestini fault, and occurred ~15 km to the north-west (Figure 1a). The Roccapreturo fault system is the nearest fault along-strike from the Paganica San Demetrio Ne Vestini fault, and therefore it experienced an increase in Coulomb stress of up to 0.6 bars due to the 2009 L'Aquila earthquake (Mildon et al., 2019). Another study reports a mean Coulomb stress transfer of 0.27 bar (maximum 1.89 bar) for the Middle Aterno Valley fault, which was used to calculate that the probability of an earthquake occurring in the next 50 years on this fault had increased by 0.5-1.5% (Pace et al., 2014).

Estimates of slip rate on the Roccapreturo fault vary depending on the primary data, measurement location and the time span the slip rate is measured over. The maximum Holocene-averaged slip rate of the fault is reported to be $0.8^{+0.52}_{-0.31}$ mm/yr (using topographic profiles (Faure Walker et al., 2021)). Cosmogenic studies show that the slip rate has been variable over the Holocene, with a period of quiescence/low slip rate from ~12 – 1.5 ka, followed by elevated slip rates of 5 mm/yr from 1.5 ka – present (based on the least squares solution, for further details see (Roberts et al., 2025)). Over longer (200 kyr) time scale, the slip rate is reported to be 0.4 ± 0.3mm/yr (using ^{36}Cl on triangular facets (Tesson et al.,

2021)). Over a 1 Myr time scale, the minimum slip rate is determined to be 0.23 – 0.34 mm/yr (based on the offset of dated breccias (Falcucci et al., 2015)).

Methods

We undertook detailed mapping along the Roccapreturo fault system to gather structural (strike and dip) and kinematic (trend and plunge) measurements from the bedrock fault scarp, which is well exposed along most of the length of the fault system (Figure 3). The morphology of the bedrock fault scarp and the geomorphology close to the fault scarp were also mapped. Localities were recorded using a handheld Garmin GPS, with an approximate location accuracy of ±5 m. Strike and dip was collected at all localities and averaged using Stereonet (Allmendinger et al., 2012) where multiple measurements were taken. Kinematic (trend and plunge) measurements were taken from frictional wear striae on the bedrock scarp where available, and/or calculated from strike and dip measurements measured around corrugations on the fault scarp. Some structural data has previously been published (Faure Walker et al., 2021; Mildon, 2017; Mildon et al., 2019), but we have gathered additional data that is previously unpublished as part of this study.

We collected nine topographic profiles across the bedrock fault scarp at locations with favourable geomorphology to calculate the Holocene throw and thus throw and slip rates, given the evidence that the hillsides stabilised at the Last Glacial Maximum (LGM, 15 ± 3kyrs (Cowie et al., 2017; Giraudi & Frezzotti, 1997)). The locations of topographic profiles were carefully selected in the field to avoid any areas of post-LGM sedimentation or erosion, for example gullies or alluvial fans, and were taken wherever the geomorphology and access (e.g. limited vegetation) were suitable. Topographic profiles were taken using two methods. Firstly, profiles were created using a 1 m ruler and a clinometer to measure the inclination of the slope, using chain-surveying techniques to cover the upper (footwall) slope, the fault scarp (both degraded and well preserved) and the lower (hanging wall) scarp. Secondly, a hand-held Trupulse and a target was used to collect vertical and horizontal positions along a transect across the fault scarp. For both methods, the local slip vector was used to orient the profile. Geomorphic features along the profile were noted, including the upper slope, the degraded fault scarp, the fault plane, the colluvial wedge (if present), and the lower slope.

The resulting profiles from both methods are then interpreted to find the line of the upper and lower slopes (using the geomorphic features recorded while surveying), and the dip of the fault plane is taken from field measurements. These interpretations give the Holocene throw values which are reported herein. We integrate our measurements with three Holocene throw values that have already been published (Faure Walker et al., 2019; Mildon et al., 2019).

We have constructed seven geological cross-sections approximately perpendicular to the strike of the Roccapreturo fault system, based on published geological maps (Servizio Geologico d'Italia, 2009b, 2009c, 2009a, 2009d). We use these cross-sections to determine the geological throw across the three strands of the Roccapreturo fault system.

To understand how strain is being accommodated by the multiple strands of the Roccapreturo fault system, we calculate the strain rate for a series of transects with variable widths, using field measurements (fault plane dip, slip vector trend and plunge), strike from simplified fault geometries generated by the chosen transect widths, and Holocene throw. We use the method developed by (Faure Walker et al., 2009, 2010, 2012), which is an adaption of (Kostrov, 1974) equations. The maximum horizontal strain-rate component of the strain rate tensor is calculated using Equation 1 (Faure Walker et al., 2010):

$$\dot{\varepsilon}_{1\prime 1\prime} = \frac{1}{2at}\sum_{k=1}^{K}\left\{L^k T^k cotp^k \left[sin(\phi^k - \Phi^k) + sin\left(\phi^k + \Phi^k + arctan\left(\frac{\sum_{k=1}^{K} L^k T^k cotp^k cos(\phi^k + \Phi^k)}{\sum_{k=1}^{K} L^k T^k cotp^k sin(\phi^k + \Phi^k)}\right)\right)\right]\right\}$$

Where $\dot{\varepsilon}_{1\prime 1\prime}$ is the maximum horizontal component of the average strain tensor, Φ = strike, ϕ = slip direction, p = plunge, T = throw, L = length of the fault, a = surface area of the region concerned, t = time during which the total slip from all the earthquakes occurred on a given fault, k = measurements for each section of the fault within the surface area. We use a range of different transect widths, 0.5, 1 and 2 km, to explore how the calculated strain varies depending on the resolution of the calculations, and to study how strain varies along a well-mapped relay zone.

Results

The Roccapreturo fault trace is well constrained along most of its 8 km length by the presence of a bedrock fault scarp (Figure 3), facilitating the collection of high resolution structural data was collected and is plotted in Figure 4. The scarp morphology and geomorphology was mapped and is shown as a series of maps in Figure 5 and Supplementary Figures 1 – 9, the exception is a section at the north-western end where the fault exposure was more sporadic and therefore it could not be mapped to the same resolution as the rest of the fault. The Middle Aterno Valley West and Succiano Faults are less well-exposed in the field, and thus there is less structural data associated with them and no mapping was undertaken.

The structural maps of the Roccapreturo fault (Figure 5, Supplementary Figures 1 – 9) show the complexity of the fault trace when mapped at 10s m resolution. The maps show the degree of preservation of the bedrock fault scarp and the extent of the well-preserved free face. The local geomorphology, including gullies, alluvial cones, drainage channels, as well as well-preserved Last Glacial Maximum surfaces in limestone (i.e. upper slope/footwall) and colluvium (i.e. lower slope/hangingwall) are recorded on the maps. These maps demonstrate that there are a number of small steps in the fault trace (Figure 5, Supplementary Figure 3, 6, 7 & 9)

The orientation and slip vector of the Roccapreturo fault system shows wide variation in the strike, dip and slip vector trend (Figure 4a-c, Supplementary Data 10). Along the whole fault system, the strike of the bedrock fault scarp varies from 072° – 183°. There is wide scatter in the graph which shows that much of the variation in strike occur over length scales of 100s of metres, rather than indicating the presence of kilometer-scale fault bend(s) (Figure 4b). The dip of the faults is also variable, from 42° – 82° °, with similar levels of short-length scale scatter observed in dip to that seen in strike (Figure 4c). The slip vectors show a broad pattern of convergence towards the centre of the fault (Figure 4a), similar to other examples of normal faulting from central Italy (Faure Walker et al., 2009; Roberts, 2007; Roberts & Michetti, 2004; Wilkinson et al., 2015).

Within the relay zone between the Roccapreturo and Succiano fault strands, the strike of both faults are within the same range (approximately 110° – 160°) and the slip vectors are

approximately parallel on both faults (Figure 4a). There are some systematic larger-scale variations in fault geometry observed, particularly in the dip of the faults. East of the relay zone where the Roccapreturo fault is isolated across-strike (i.e. no other fault strands across-strike, from 5 – 10 km, Figure 4), the average dip of the fault is lower (56.4 ± 0.4°) than in the relay zone, with average dips of 65.7 ± 0.7°, 75.2 ± 1.9° and 59.1 ± 0.1° for the Roccapreturo, Succiano and Middle Aterno Valley West faults respectively (Figure 4c). Where the Middle Aterno fault is isolated across-strike (from 0 – 2 km, Figure 4), the average dip is lower (52.9 ± 0.4°) than in relay zone. Overall, the fault system has a lower dip when there is a single across-strike fault, and the dip is steeper where the fault strands overlap.

In total, twelve Holocene throw profiles have been gathered along these faults (Figure 2b, 4d, (Faure Walker et al., 2019; Mildon et al., 2019)). Each strand of the Roccapreturo fault system has at least one Holocene throw measurement. The Holocene throw has been estimated by eye in the field at two other locations, for these, the assigned error is ±50% of the throw. The maximum Holocene throw recorded along the fault is 8.75 ± 1.75 m, which corresponds to a Holocene throw rate of 0.58 ± 0.16 mm/yr (Figure 4d). The cumulative Holocene throw profile for the fault system does not show a single clear peak in the middle of the fault which may be expected assuming a triangular or bell-shaped throw profile (Cowie & Scholz, 1992; Manighetti et al., 2004; Manzocchi et al., 2006; Nicol et al., 2005; Roberts, 2007). Minima are observed at the transfer zones between the different faults.

Seven geological cross-sections were constructed across the Roccapreturo fault system, with a minimum of two cross-sections on each of the three fault traces (Supplementary Figure 11) to measure the geological throw. The cumulative geological throw profile for the fault system shows a more typical throw profile expected for a normal fault (Figure 4e). The maximum cumulative geological throw across the Roccapreturo fault system is 610 m.

Strain rate calculations

For the purposes of the strain rate calculations, we choose to omit the Santa Maria Del Ponte West trace from the Middle Aterno Valley West fault, because 1) this trace has the lowest activity and location scale of all the traces in the Roccapreturo fault system (Figure 2a), which means it is poorly constrained, and 2) there are Plio-Pleistocene deposits in both the footwall and hangingwall of the Santa Maria Del Ponte West trace, implying limited

geological offset (Supplementary Figure 11), supported by the geological throw profile (Figure 4e), 3) it creates a sharp bend with the Middle Aterno Valley West trace of ~140° which may be unrealistic, and 4) we do not have any structural or throw data along this trace.

Given the high resolution of structural and throw rate data gathered along the Roccapreturo fault system, and in particular the Roccapreturo fault, we can calculate the strain rate across the fault system for a range of scales. We present the strain rate calculated for three different transect widths, 500 m, 1 km and 2 km (Figure 6). All three transects show a similar pattern of strain rate along the length of the fault (Figure 6a), with the maximum strain rate located approximately 9 km along strike, skewed towards the south-eastern tip of the fault. Interestingly, the strain rate profile is smoother than the Holocene throw rate profile for the three faults (Figure 4d), implying that the geometry and the throw are co-varying to create a smooth strain rate profile.

Based on the distribution and resolution of the throw rate data gathered, our preferred transect width is 1 km as then almost all transects have at least one measurement of Holocene throw, therefore for this transect width, we also show the orientation of the maximum horizontal strain rate (Figure 6b). The orientation shows a broad pattern of convergence, following the convergence in the slip vector (Figure 4a).

Discussion

Proposed changes of fault traces

Based on our field data gathered, we would propose the following changes to the Fault2SHA database, and other Italian fault databases, e.g. the ITHACA database. 1) Adjust the trace of the Beffi trace to match the localities gathered (Supplementary Figure 12), 2) Increase the location scale to level 1 and the activity scale to level 2 for the Beffi trace because a bedrock fault scarp has been ground truthed along the trace and a Holocene throw profile has been collected (Supplementary Figure 12), 3) The section of the Roccapreturo North West trace with additional field data should be changed to a location scale of 1 because a bedrock fault scarp has been ground truthed along the trace and activity scale of 1 (dated displacement during the Late Pleistocene/Holocene) **or** the Roccapreturo Acciano trace should be extended to the north-west. Furthermore, the shape of the geological throw profile (Figure

4e) shows a typical bell- or triangular shape expected for normal faults, implying that the three strands as we map them (i.e. removing the Santa Maria del Ponte trace, and shortening the Middle Aterno Valley West fault) are a) behaving as a single main fault and b) include the tips of the fault. Therefore, based on the shape of the geological throw profile, we would suggest that the Middle Aterno Valley Main Fault is split in two in the Fault2SHA database.

Structural maturity and sub-surface connectivity of the Roccapreturo fault zone

The geometry (strike and dip) of the Roccapreturo fault system is highly variable at short (~100s m) length scales. Previous studies have suggested that the level of corrugation (i.e. variations in the fault strike) and segmentation decreases as a fault becomes more mature (e.g. Brodsky et al., 2011; Manighetti et al., 2021; Sagy et al., 2007). Manighetti et al. (2021) suggest that the standard deviation of fault strike (which they call "fault gradient") is high for immature faults, with the smallest window length giving standard deviations of 14 – 24° for the immature faults studied. In our study, the standard deviation of locality-averaged strike measurements for the Roccapreturo fault system is 18°. Although direct comparison of our results to those of (Manighetti et al., 2021) is not possible, because their results are calculated for faults longer than 40 km (i.e. far longer than the Roccapreturo fault system) and because they calculate the standard deviation of strike from the fault trace, the similarity of the results let us suggest that the Roccapreturo fault system should be considered as an immature fault. Furthermore, there are several small (< 100 m) relay zones along the mapped fault trace (Figure 5, Supplementary Figure 3, 6, 7, 8), as well as the relay zone formed by the Middle Aterno Valley West, Succiano and Roccapreturo faults, demonstrating segmentation at a range of scales and thus also indicating low structural maturity of the fault.

The geometry-dependent throw rate model developed in the Central Apennines (Faure Walker et al., 2019) implies that there will be a greater throw and steeper dip within a fault bend in order to maintain the strain rate across the faults. Our observations from the Roccapreturo fault system show that there are steeper dips where there is overlap between the three different faults (~3 – 5 km distance, Figure 4c), and that there is the cumulative

Holocene throw maximum within this section of the fault (Figure 4d). Importantly, the slip vector across the relay zone (i.e. incipient bend) is consistent, which is required for the geometry-dependent throw rate model to be applicable. From this, we interpret that, where the faults overlap at the surface, in the sub-surface the faults are connected, forming a fault bend with steeper dip than the isolated sections of the fault (Figure 8). This is supported by the convergence of slip vectors along the length of the fault, which has previously been recognised to be an indication that separate surface faults are connected in the sub-surface (Faure Walker et al., 2009; Roberts, 2007; Roberts & Michetti, 2004; Wilkinson et al., 2015).

The shape of the geological throw profile (Figure 4e) shows the expected triangular to bell shape expected for normal faults (Cowie & Scholz, 1992; Manighetti et al., 2004; Manzocchi et al., 2006; Nicol et al., 2005; Roberts, 2007), with a maxima in approximately the middle of the fault that tapers towards zero at the tips. This implies that the three fault strands are kinematically linked and may be hard-linked together at depth. The maximum throw on the Roccapreturo fault system is 610 m. To compare this value with other faults in the region, we have compiled geological throw data from other normal faults in the Central Apennines from other published sources (Boncio et al., 2004; Iezzi et al., 2019; Roberts & Michetti, 2004; Schirripa Spagnolo et al., 2021; Testa et al., 2019). Note that we only include values in this compilation if the geological throw is well located along a fault, i.e. with a geological cross-section. We plot the geological throw versus the length for both the “Faults” and “Main Faults” categories as defined by the Fault2SHA database (Faure Walker et al., 2021), where more detailed local studies exist, we use their fault lengths. For both categories, the faults in the Roccapreturo fault system have some of the lowest total geological throw values in the Central Apennines (Figure 7). We also calculate the throw/length ratio using the “Main Fault” category, the Roccapreturo fault has a throw/length ratio of 0.055, this value is below average when compared to other faults in the Central Apennines (0.035 – 0.083 (Roberts & Michetti, 2004)). This may suggest that the Roccapreturo fault system has a lower degree of maturity within the central Apennine fault system.

The shape of the Holocene throw profile differs from the geological throw profile in that it does not follow a simple triangular to bell shape (Figure 4d & 8). Instead, a throw minima is located at the eastern edge of the relay zone between the Roccapreturo and Succiano faults. On the geological map (Supplementary Figure 11) and other papers about this fault system

(Goodall et al., 2021), there are a number of minor faults mapped in this area, although it is unclear from these maps whether these faults should be considered as Holocene active or not, and we did not find any clear evidence in the field of these minor structures. If these faults are active but had very small (< 1 m) amounts of throw that could not be readily recognised in the field, this may explain why the total Holocene throw is low at this point. Similar observations have been made for small-scale relay structures, where it is noted that there was a change from localised to distributed deformation within a relay ramp (Nixon et al., 2019).

Taken together the structural and the geological throw data, we infer that, although the three fault strands are separate at the surface, at depth they connect and a fault bend exists in the area where the faults overlap (Figure 8). Based on this inference, we suggest that the Roccapreturo fault system is at Time 5 in the evolution of a fault bend shown in Figure 1b, with separate strands at the surface, connected together at depth.

In the future, we would anticipate that the fault bend at depth will propagate to the surface and eventually the relay zone will develop into a fault bend (i.e. like Time 6 in Figure 1b), though we cannot constrain the timescale of this process. The exact geometry of the fault bend at the surface, for example whether the Succiano fault is eventually abandoned, or how the Middle Aterno West and Roccapreturo fault join, cannot be constrained from the present field data.

Speculation on the earthquake behaviour of the Roccapreturo fault system and implications for seismic hazard

There are no earthquakes in the historical record (Guidoboni et al., 2019) that can be confidently assigned to the Roccapreturo fault system, and as there are only two paleoearthquakes recognised (Falcucci et al., 2015), it is not possible to deduce a recurrence interval from the historic/paleoseismic catalogue. Therefore, understanding the potential seismic hazard and characteristics of any earthquakes that could be generated by this fault system would be useful.

Studies have suggested that the structural maturity of faults affects the resulting earthquake behaviour, including lower stress drops (Choy & Kirby, 2004; Hecker et al., 2010; Manighetti et al., 2007), more distributed damage (Thakur & Huang, 2021) due to less efficient rupture

propagation (Andrews et al., 2026; Guo et al., 2023), more aftershocks (Guo et al., 2023), and irregular recurrence intervals (Thakur & Huang, 2021) for low maturity faults. Our results indicate that the Roccapreturo fault system is an immature fault system, because of the 1) range of strike values, 2) separate fault strands at the surface, and 3) low geological throw and T/L ratio. In addition, the Holocene slip histories inverted from ^{36}Cl cosmogenic studies (Goodall et al., 2021; Iezzi et al., 2025; Roberts et al., 2025) show variable slip rate, which could also be interpreted to be phases of clustering/anti-clustering of earthquakes, i.e. irregular recurrence intervals. The complex Holocene throw profile may also indicate more variable earthquake behaviour, i.e. full and partial ruptures and therefore a greater range of potential earthquake magnitudes and higher CoV (coefficient of variation, defined as the standard deviation of the mean recurrence time, divided by the mean recurrence time). This speculation is based on earthquake cycle models of a normal fault in central Italy driven by different throw profiles (Rodriguez Piceda et al., 2025). Furthermore, within relay zones it is expected that there will be more distributed or off-fault coseismic damage (e.g. 50% strain accommodated by off-fault damage from a small-scale study (Nixon et al., 2019). Dissipative processes such as fracture formation and gouge production on subsidiary faults within a wide damage zone significantly contribute to the earthquake energy budget (Cocco et al., 2023; Okubo et al., 2019) by reducing the amount of energy available for rupture propagation (Shipton et al., 2006).

There are two competing factors that will affect the magnitude of earthquakes generated on the Roccapreturo fault system. The rupture area of a connected fault will be larger than three separate faults (i.e. if the surface geometry was extended to depth), which would imply larger earthquakes based on scaling laws (Wells & Coppersmith, 1994). However, the presence of a fault bend may inhibit rupture propagation if an earthquake was to nucleate on either the north-west or south-eastern end of the Roccapreturo fault system (Biasi & Wesnousky, 2016; Manighetti et al., 2007; Mildon et al., 2017; Steacy & McCloskey, 1998), thus limiting the magnitude of the resulting earthquake. Therefore, we might expect that future earthquakes on this fault will have low stress drops, wider damage zones and/or distributed ruptures, more aftershocks, and more irregular recurrence intervals.

Conclusions

The Roccapreturo fault system is well-exposed at the surface by carbonate bedrock scarps, and thus abundant structural and throw data can be gathered along its length. At present, the fault system is comprised of three separate fault strands at the surface. Through combining collected structural data and Holocene and geological throw data, we hypothesise that these three surface strands are connected together in the sub-surface, based on 1) the convergence of slip vectors, 2) steeper dips in the relay zone between the strands and 3) the shape of the geological throw profile. Therefore, this also implies that the Roccapreturo fault system is a relatively immature fault, which is supported by the wide range of fault geometry, a relatively low geological throw and T/L ratio compared to other normal faults in the Central Apennines. The complex fault geometry and sub-surface connectivity is important to document, particularly constraining that the faults are connected in the sub-surface, as longer faults produce larger earthquakes. However, as there are no historical earthquakes related to this fault, we do not know how an earthquake would propagate through the disconnected surface fault system. We speculate that the disconnected surface fault system with high variability in the fault geometry may result lower stress drops, wider damage zones and/or distributed ruptures, more aftershocks, and more irregular recurrence intervals. Our study confirms the value in conducting high-spatial resolution geological mapping of normal fault scarps to constrain the activity, connectivity and seismic potential of active faults.

Acknowledgements

This work was funded by UK Research and Innovation (UKRI) under the auspices of the project Quake4D MR/T041994/1 (Z. Mildon), NERC Standard Grant NE/I024127/1 (G. Roberts), and NERC Studentship NE/L501700/1 (Z. Mildon). Luke Wedmore is thanked for field assistance.

Figures

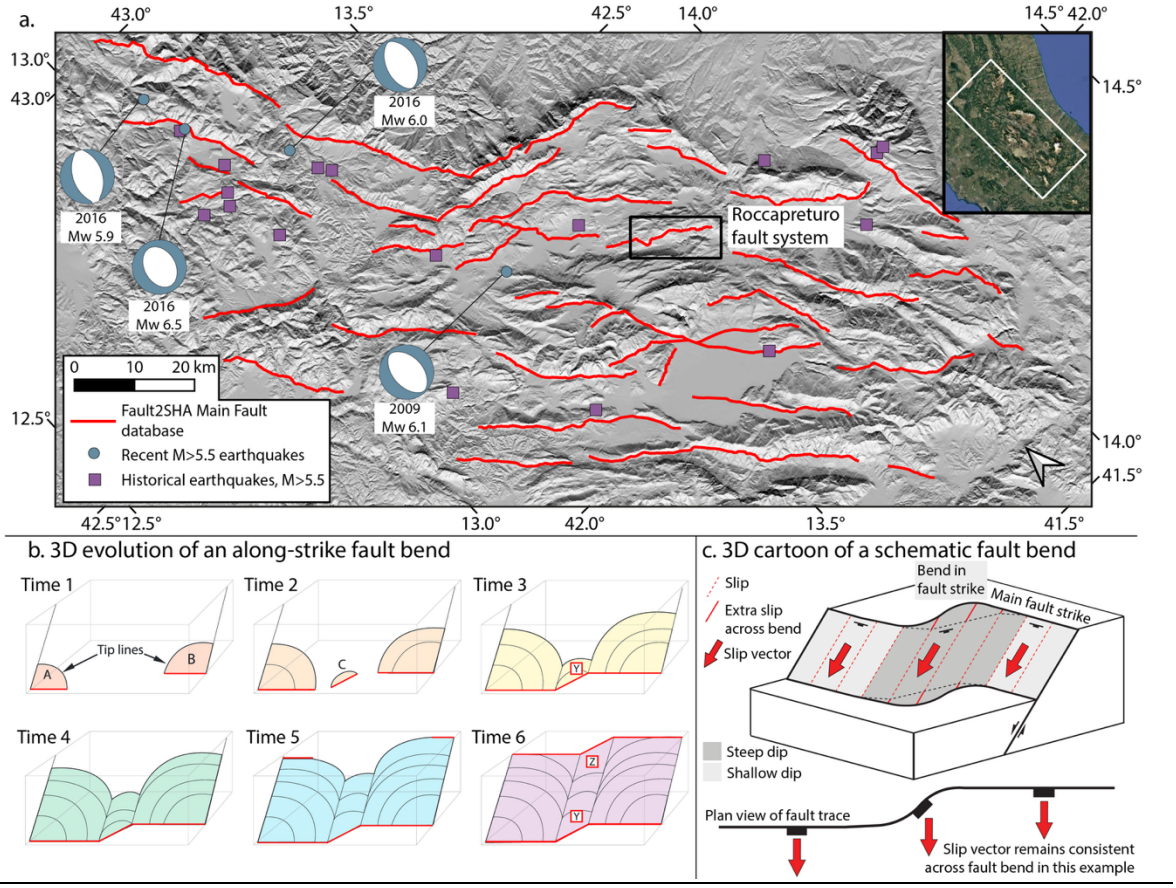

Figure 1 – Location and scientific overview of the study area. a) Fault map of the Central Apennines using the "Main Faults" from the Fault2SHA database (Faure Walker et al., 2021). Recent earthquake locations and focal mechanisms with M>5.5 are shown in blue circles (ISIDe Working Group, 2007). Historical earthquake locations are shown with purple squares (Guidoboni et al., 2019). DEM is from TINITALY (Tarquini et al., 2012). Inset map shows the location within Italy, imagery from Google Earth. Black box indicates the location of the studied Roccapreturo fault system. b) Schematic diagram of a 3D evolution from an along-strike fault bend by propagation of en-echelon faults and eventual linkage (adapted from (Iezzi et al., 2018)). The along strike bend (C) forms at depth (Y) earlier than at the surface (Z), and these bends typically have steeper dips. c) geometry-dependent throw-rate model (Faure Walker et al., 2019), which implies that the throw and dip vary throughout along-strike fault bends to keep the strain-rate concomitant.

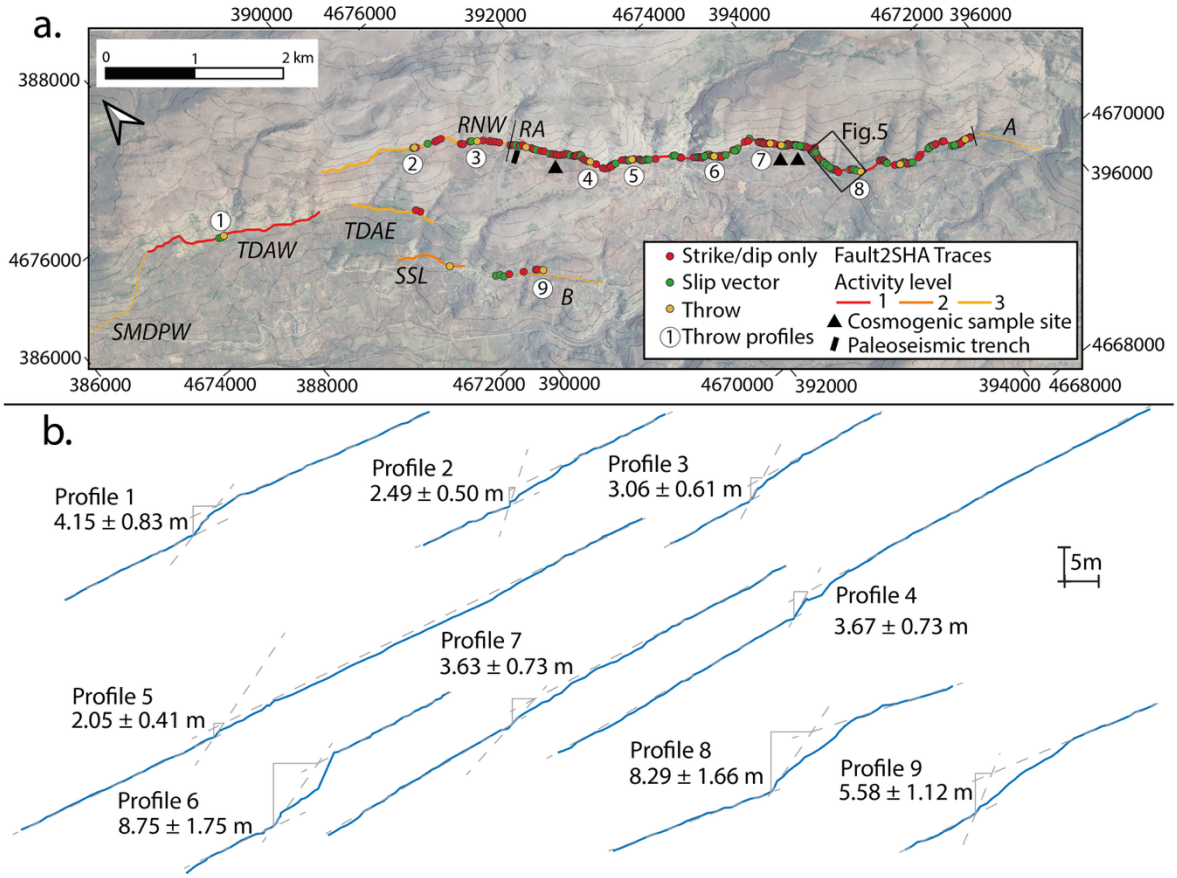

Figure 2 – a) Map of the gathered data plotted onto the Fault2SHA Traces (Faure Walker et al., 2021), colour coded according to activity level (1- dated Holocene displacement, 2- evidence of Holocene displacement, 3- geologic or geomorphic evidence of fault activity). SMDPW – Santa Maria Del Ponte West trace, TDAW – Tione Degli Abruzzi West trace, TDAE – Tione Degli Abruzzi East trace, SSL – Succiano San Lorenzo trace, B – Beffi trace, RNW – Roccapreturo North West trace, RA – Roccapreturo Acciano trace, A – Acciano trace. Coloured dots correspond to the level of data gathered, all locations have a strike and dip, some locations have the slip vector measured, and some locations have a Holocene throw profile taken. Black rectangle shows the location of the paleoseismic trench (Falcucci et al., 2015). Black triangles show the cosmogenic sample sites (Goodall et al., 2021; Roberts et al., 2025). Black box shows the extent of the structural map in Figure 5. b) Previously unpublished Holocene throw profiles are plotted at the same scale (no vertical exaggeration), and labelled 1 – 9, their locations are indicated on the map with numbers in circles.

Figure 3 – Field photographs showing the geomorphology of the bedrock fault scarp. a) wide angle view of a southern section of the Roccapreturo fault, b) upstanding fault scarp where the immediate footwall has been eroded away, c) bedrock scarp with a small alluvial cone on the hangingwall, d) striated fault scarp with minimal erosion, e) view along the fault scarp into a gully.

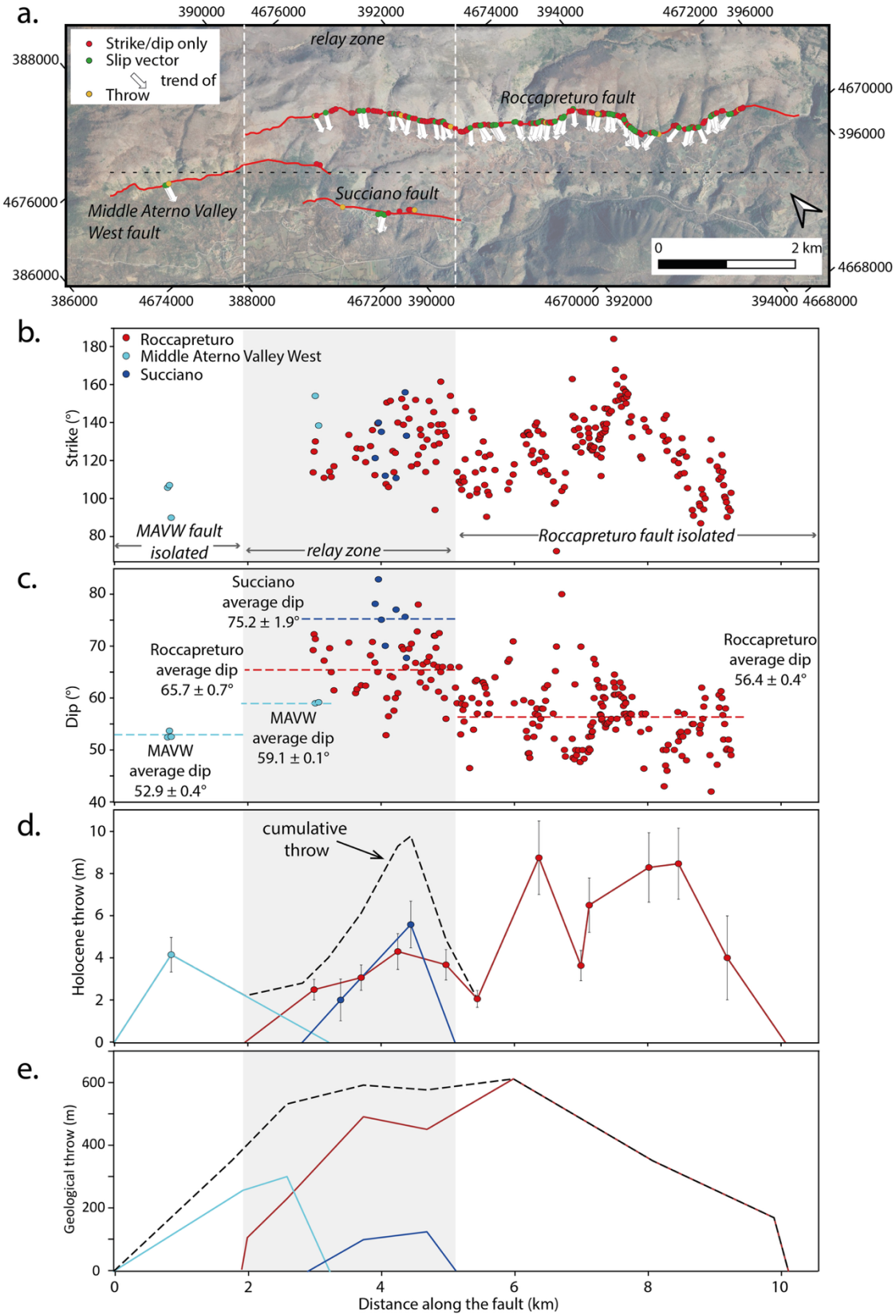

Figure 4 – Structural and throw data gathered along the Roccapreturo fault system. a) overview of the locations of collected data, colour coded according to the type of data collected. White arrows show the trend of slip vector data collected, which broadly show

519 convergence. Faults and the extent of the relay zone between faults are labelled. Sub-plots
520 show the b) strike, c) dip, d) Holocene throw and e) geological throw plotted along distance
521 along the fault, colour coded according to the associated fault. The extent of the relay zone
522 between faults is shown in grey. When averaged based on location, the dips of the faults in
523 the relay zone are higher than the dips of the faults when there is no across-strike
524 overlapping fault.

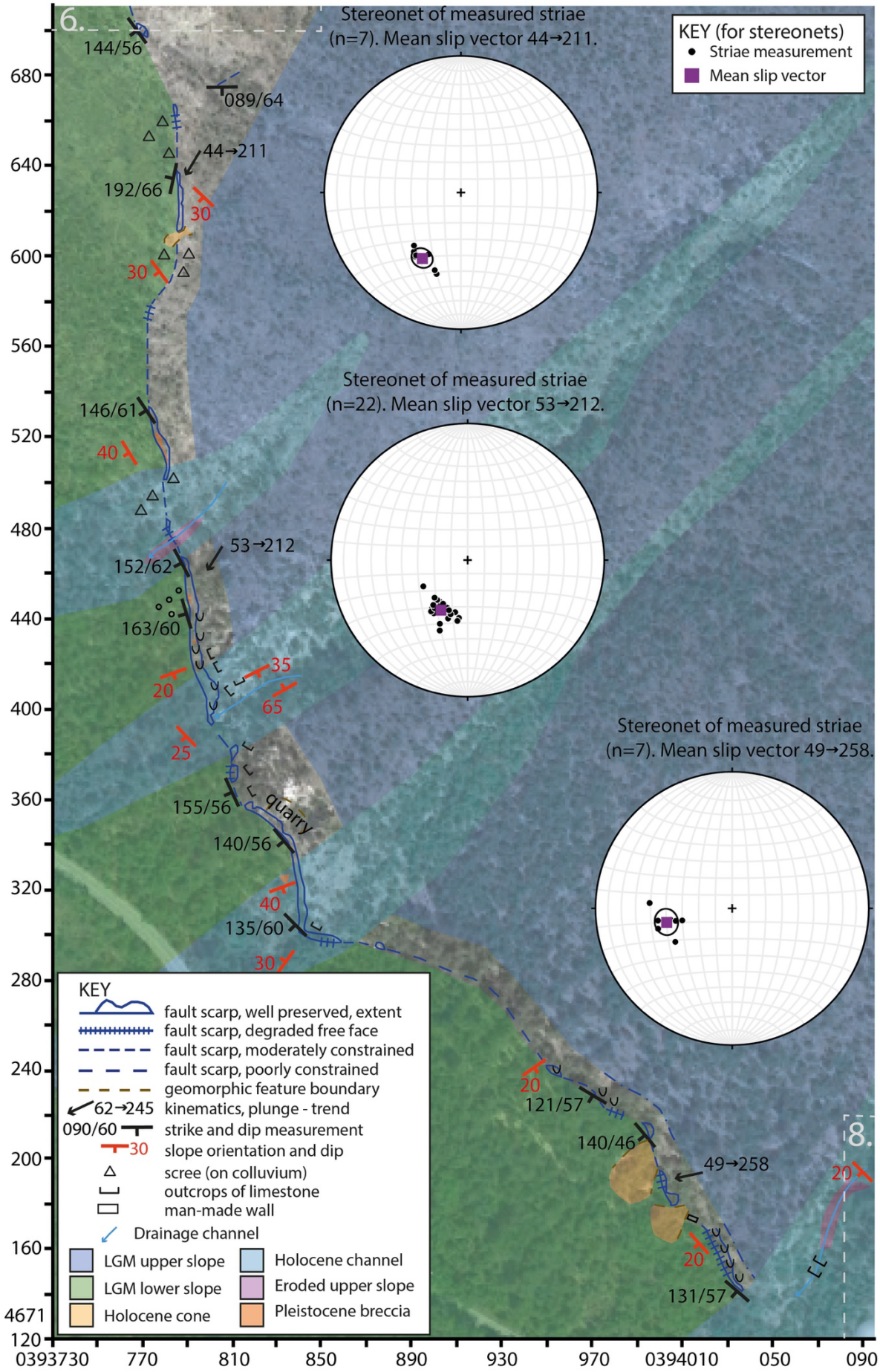
6.
8.
Stereonet of measured striae
(n=7). Mean slip vector 44→211.
KEY (for stereonets)
Striae measurement
Mean slip vector
Stereonet of measured striae
(n=22). Mean slip vector 53→212.
Stereonet of measured striae
(n=7). Mean slip vector 49→258.
144/56
089/64
44→211
192/66
30
30
146/61
40
53→212
152/62
163/60
20
35
65
25
155/56
quarry
140/56
40
135/60
30
20
121/57
140/46
49→258
20
20
131/57
KEY
fault scarp, well preserved, extent
fault scarp, degraded free face
fault scarp, moderately constrained
fault scarp, poorly constrained
geomorphic feature boundary
62→245 kinematics, plunge - trend
090/60 strike and dip measurement
30 slope orientation and dip
scree (on colluvium)
outcrops of limestone
man-made wall
Drainage channel
LGM upper slope
LGM lower slope
Holocene cone
Holocene channel
Eroded upper slope
Pleistocene breccia
680
640
600
560
520
480
440
400
360
320
280
240
200
160
120
4671
0393730
770
810
850
890
930
970
0394010
050
090

Figure 5 – Example structural map of a section of the Roccapreturo fault, location of this map is shown in Figure 2. The preservation and morphology of the bedrock fault scarp is mapped. Structural data (strike/dip of the fault plane and trend/plunge of slip vector) is collected and plotted, stereonets show the average trend/plunge of slip vector where multiple frictional wear striations are collected at a single locality. Background is Google Earth imagery. Coordinates given are UTM zone 33N. Grey dashed boxes and numbers indicate the overlap with subsequent structural maps (shown in Supplementary Figures 1-10).

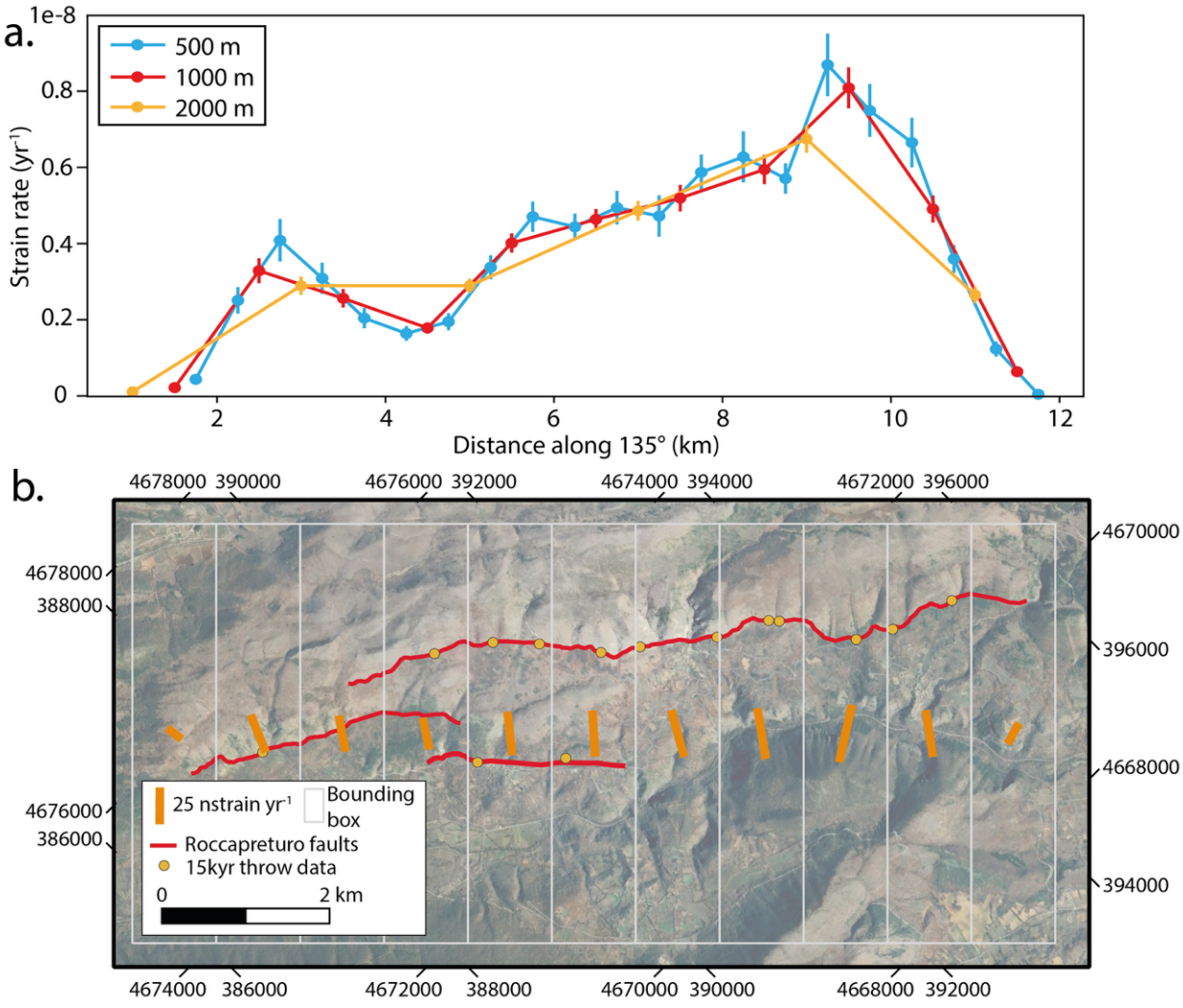

Figure 6 – Strain rate calculations across the Roccapreturo fault system. a) Strain rate across the Roccapreturo fault system (i.e. across all three fault strands), calculated for three different width bounding boxes. b) Strain rate calculated for 1 km wide bounding boxes,

539 showing the orientation and magnitude of the principal horizontal strain rate. Transects that
540 are 1 km wide are chosen as, at this resolution, the majority of transects include at least one
541 measurement of Holocene throw.

542

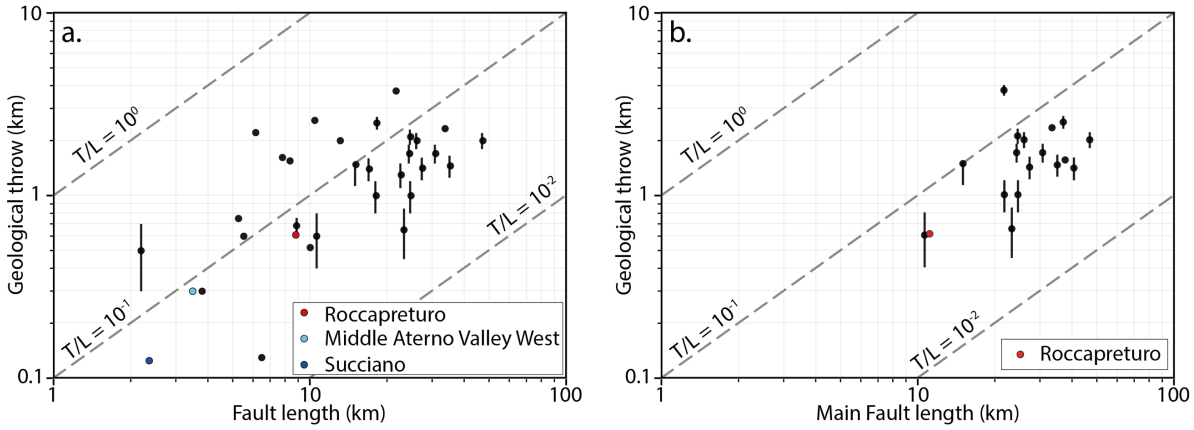

543

544 Figure 7 – Geological throw compilation from the Central Apennines. a. Geological throw
545 versus fault length for the "Fault" level from the Fault2SHA database (Faure Walker et al.,
546 2021). The three fault strands of the Roccapreturo fault system are highlighted. b. Geological
547 throw versus fault length for the "Main Fault" level from the Fault2SHA database. Geological
548 throw data compiled from a range of sources (Boncio et al., 2004; Iezzi et al., 2019; Roberts
549 & Michetti, 2004; Schirripa Spagnolo et al., 2021; Testa et al., 2019).

550

551

552

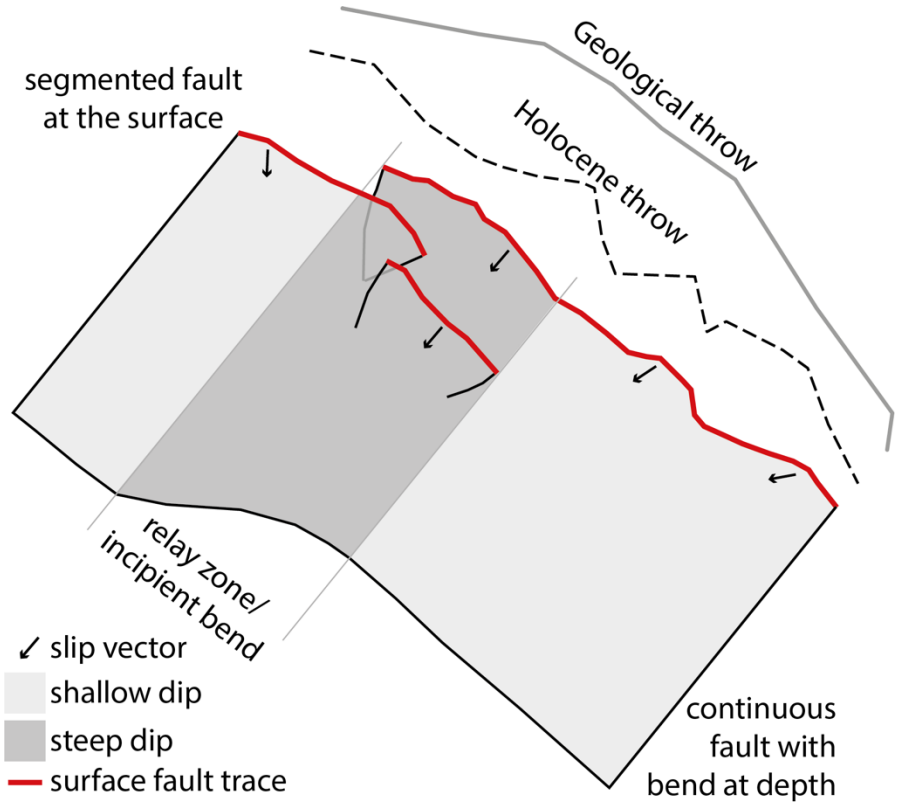

Figure 8 – Cartoon of the hypothesised structure of the Roccapreturo fault system (not-to-scale), showing the separate fault strands at the surface and the hypothesised fault bend at depth. The cumulative geological and Holocene throw profiles are also shown, as well as indicative convergent slip vectors.

References

Alessio, G., Alfonsi, L., Brunori, C. A., Cinti, F. R., Civico, R., Cucci, L., et al. (2010). Evidence for Surface rupture associated with the Mw 6.3 L'Aquila earthquake sequence of April 2009 (central Italy). *Terra Nov.*, *22*(1), 43–51. https://doi.org/10.1111/j.1365-3121.2009.00915.x

566 Allen, J. R. M., Huntley, B., Brandt, U., Brauer, A., Hubberten, H.-W., Keller, J., et al.
567 (1999). Rapid environmental changes in southern Europe during the last glacial
568 period. *Nature*, *400*(6746), 740–743. https://doi.org/10.1038/23432
569 Allmendinger, R. W., Cardozo, N., & Fisher, D. M. (2012). *Structural Geology Algorithms:*
570 *Vectors and tensors* (1st ed.). Cambridge University Press.
571 Anderson, H., & Jackson, J. A. (1987). Active tectonics of the Adriatic Region.
572 *Geophysical Journal International*, *91*, 937–983.
573 Andrews, B. J., Piceda, C. R., Peacock, D. C. P., & Mildon, Z. K. (2026). Interplay between
574 geometry and brittle deformation of bedrock fault scarps. Retrieved from
575 https://eartharxiv.org/repository/view/11981/
576 Biasi, G. P., & Wesnousky, S. G. (2016). Bends and Ends of Surface Ruptures. *Bulletin of*
577 *the Seismological Society of America*, (2009).
578 https://doi.org/10.1785/0120160292
579 Boncio, P., Lavecchia, G., Milana, G., & Rozzi, B. (2004). Seismogenesis in Central
580 Apennines , Italy: an integrated analysis of minor earthquake sequences and
581 structural data in the Amatrice-Campotosto area. *Annals of Geophyics*,
582 *47*(December), 1723–1742.
583 Brodsky, E. E., Gilchrist, J. J., Sagy, A., & Collettini, C. (2011). Faults smooth gradually as
584 a function of slip. *Earth and Planetary Science Letters*, *302*(1), 185–193.
585 https://doi.org/10.1016/j.epsl.2010.12.010
586 Carminati, E., Lustrino, M., & Doglioni, C. (2012). Geodynamic evolution of the central
587 and western Mediterranean: Tectonics vs. igneous petrology constraints.
588 *Tectonophysics*, *579*, 173–192. https://doi.org/10.1016/j.tecto.2012.01.026

589 Cartwright, J. A., Trudgill, B. D., & Mansfield, C. S. (1995). Fault growth by segment
590 linkage: an explanation for scatter in maximum displacement and trace length
591 data from the Canyonlands Grabens of SE Utah. *Journal of Structural Geology*,
592 *17*(9), 1319–1326. https://doi.org/10.1016/0191-8141(95)00033-A
593 Cavinato, G. P., & De Celles, P. G. (1999). Extensional basins in the tectonically bimodal
594 central Apennines fold-thrust belt , Italy : Response to corner flow above a
595 subducting slab in retrograde motion. *Geology*, *27*(10), 955–958.
596 Choy, G. L., & Kirby, S. H. (2004). Apparent stress, fault maturity and seismic hazard for
597 normal-fault earthquakes at subduction zones. *Geophysical Journal*
598 *International*, *159*(3), 991–1012. https://doi.org/10.1111/j.1365-
599 246X.2004.02449.x
600 Cocco, M., Aretusini, S., Cornelio, C., Nielsen, S. B., Spagnuolo, E., Tinti, E., & Toro, G. D.
601 (2023). Fracture Energy and Breakdown Work During Earthquakes. *Annual*
602 *Review of Earth and Planetary Sciences*, *51*(Volume 51, 2023), 217–252.
603 https://doi.org/10.1146/annurev-earth-071822-100304
604 Cowie, P. A., & Scholz, C. H. (1992). Displacement-length scaling relationship for faults:
605 data synthesis and discussion. *Journal of Structural Geology*, *14*(10), 1149–1156.
606 https://doi.org/10.1016/0191-8141(92)90066-6
607 Cowie, P. A., Phillips, R. J., Roberts, G. P., McCaffrey, K. J. W., Zijerveld, L. J. J., Gregory, L.
608 C., et al. (2017). Orogen-scale uplift drives episodic behaviour of earthquake
609 faults. *Nature Scientific Reports*, (November 2016), 1–10.
610 https://doi.org/10.1038/srep44858
611 D'Agostino, N., Mantenuto, S., D'Anastasio, E., Giuliani, R., Mattone, M., Calcaterra, S.,
612 et al. (2011). Evidence for localized active extension in the central Apennines

(Italy) from global positioning system observations. *Geology*, *39*(4), 291–294. https://doi.org/10.1130/G31796.1

DePolo, C. M., Clark, D. G., Slemmons, D. B., & Ramelli, A. R. (1991). Historical surface faulting in the Basin and Range province, western North America: implications for fault segmentation. *Journal of Structural Geology*, *13*(2), 123–136. https://doi.org/10.1016/0191-8141(91)90061-M

Falcucci, E., Gori, S., Moro, M., Fubelli, G., Saroli, M., Chiarabba, C., & Galadini, F. (2015). Deep reaching versus vertically restricted Quaternary normal faults: Implications on seismic potential assessment in tectonically active regions: Lessons from the middle Aterno valley fault system, central Italy. *Tectonophysics*, *651–652*, 186–198. https://doi.org/10.1016/j.tecto.2015.03.021

Faure Walker, J. P., Roberts, G. P., Cowie, P. A., Papanikolaou, I. D., Sammonds, P. R., Michetti, A. M., & Phillips, R. J. (2009). Horizontal strain-rates and throw-rates across breached relay zones, central Italy: Implications for the preservation of throw deficits at points of normal fault linkage. *Journal of Structural Geology*, *31*(10), 1145–1160. https://doi.org/10.1016/j.jsg.2009.06.011

Faure Walker, J. P., Roberts, G. P., Sammonds, P. R., & Cowie, P. A. (2010). Comparison of earthquake strains over 10^{2} and 10^{4} year timescales: Insights into variability in the seismic cycle in the central Apennines, Italy. *Journal of Geophysical Research*, *115*(B10), B10418. https://doi.org/10.1029/2009JB006462

Faure Walker, J. P., Roberts, G. P., Cowie, P. A., Papanikolaou, I. D., Michetti, A. M., Sammonds, P. R., et al. (2012). Relationship between topography, rates of extension and mantle dynamics in the actively-extending Italian Apennines.

637 *Earth and Planetary Science Letters*, *325–326*, 76–84.
638 https://doi.org/10.1016/j.epsl.2012.01.028
639 Faure Walker, J. P., Roberts, G. P., Cowie, P. A., Mccaffrey, K. J. W., Wedmore, L., Watson,
640 Z. K., & Gregory, L. C. (2015). Long-term strain rates as a tool for understanding
641 the mechanics of continental extension and the importance of local 3D fault
642 geometry for local throw-rates across faults. In *INQUA Focus Group on*
643 *Paleoseismology and Active Tectonics*.
644 Faure Walker, J. P., Visini, F., Roberts, G. P., Galasso, C., McCaffrey, K., & Mildon, Z.
645 (2019). Variable fault geometry suggests detailed fault-slip-rate profiles and
646 geometries are needed for fault-based probabilistic seismic hazard assessment
647 (PSHA). *Bulletin of the Seismological Society of America*, *109*(1).
648 https://doi.org/10.1785/0120180137
649 Faure Walker, J. P., Boncio, P., Pace, B., Roberts, G. P., Benedetti, L., Scotti, O., et al.
650 (2021). Fault2SHA Central Apennines database and structuring active fault data
651 for seismic hazard assessment. *Scientific Data*, *8*(1), 87.
652 https://doi.org/10.1038/s41597-021-00868-0
653 Galadini, F., & Galli, P. (2000). Active Tectonics in the Central Apennines (Italy)– Input
654 Data for Seismic Hazard Assessment. *Natural Hazards*, *22*, 225–270.
655 Giba, M., Walsh, J. J., & Nicol, A. (2012). Segmentation and growth of an obliquely
656 reactivated normal fault. *Journal of Structural Geology*, *39*, 253–267.
657 https://doi.org/10.1016/j.jsg.2012.01.004
658 Giraudi, C., & Frezzotti, M. (1997). Late Pleistocene Glacial Events in the Central
659 Apennines , Italy. *Quaternary Research*, *290*(48), 280–290.

660 Goodall, H. J., Gregory, L. C., Wedmore, L. N. J., McCaffrey, K. J. W., Amey, R. M. J.,
661 Roberts, G. P., et al. (2021). Determining Histories of Slip on Normal Faults With
662 Bedrock Scarps Using Cosmogenic Nuclide Exposure Data. *Tectonics*, *40*(3),
663 e2020TC006457. https://doi.org/10.1029/2020TC006457
664 Guidoboni, E., Ferrari, G., Tarabusi, G., Sgattoni, G., Comastri, A., Mariotti, D., et al.
665 (2019). CFTI5Med, the new release of the catalogue of strong earthquakes in Italy
666 and in the Mediterranean area. *Scientific Data*, *6*(1), 80.
667 https://doi.org/10.1038/s41597-019-0091-9
668 Guo, H., Lay, T., & Brodsky, E. E. (2023). Seismological Indicators of Geologically
669 Inferred Fault Maturity. *Journal of Geophysical Research: Solid Earth*, *128*(10),
670 e2023JB027096. https://doi.org/10.1029/2023JB027096
671 Hayek, J. N., Marchandon, M., Li, D., Pousse-Beltran, L., Hollingsworth, J., Li, T., &
672 Gabriel, A.-A. (2024). Non-Typical Supershear Rupture: Fault Heterogeneity and
673 Segmentation Govern Unilateral Supershear and Cascading Multi-Fault Rupture
674 in the 2021 {M_w\7.4 Maduo Earthquake. *Geophysical Research Letters*, *51*(20),
675 e2024GL110128. https://doi.org/10.1029/2024GL110128
676 Hecker, S., Dawson, T. E., & Schwartz, D. P. (2010). Normal-Faulting Slip Maxima and
677 Stress-Drop Variability: A Geological Perspective. *Bulletin of the Seismological*
678 *Society of America*, *100*(6), 3130–3147. https://doi.org/10.1785/0120090356
679 Iezzi, F., Mildon, Z., Walker, J. F., Roberts, G., Goodall, H., Wilkinson, M., & Robertson, J.
680 (2018). Coseismic Throw Variation Across Along-Strike Bends on Active Normal
681 Faults: Implications for Displacement Versus Length Scaling of Earthquake
682 Ruptures. *Journal of Geophysical Research: Solid Earth*, *123*(11), 9817–9841.
683 https://doi.org/10.1029/2018JB016732

684 Iezzi, F., Roberts, G., Walker, J. F., & Papanikolaou, I. (2019). Occurrence of partial and
685 total coseismic ruptures of segmented normal fault systems: Insights from the
686 Central Apennines, Italy. *Journal of Structural Geology*, *126*, 83–99.
687 https://doi.org/10.1016/j.jsg.2019.05.003
688 Iezzi, F., Sgambato, C., Roberts, G., Mildon, Z., Robertson, J., Faure Walker, J., et al.
689 (2025). Structural controls on simultaneous earthquake clustering and normal
690 fault synchronization. *Earth and Planetary Science Letters*, *671*.
691 https://doi.org/10.1016/j.epsl.2025.119686
692 ISIDe Working Group. (2007). Italian Seismological Instrumental and Parametric
693 Database (ISIDe) [Data set]. https://doi.org/https://doi.org/10.13127/ISIDE
694 King, G., & Nabelek, J. (1985). Role of Fault Bends in the Initiation and Termination of
695 Earthquake Rupture. *Science*, *228*(4702), 984–987.
696 https://doi.org/http://www.jstor.org/stable/1694250
697 Kostrov, V. V. (1974). Seismic moment and energy of earthquakes, and seismic flow of
698 rock. *Earth Physics*, *1*, 23–40.
699 Manighetti, I., King, G., & Sammis, C. G. (2004). The role of off-fault damage in the
700 evolution of normal faults. *Earth and Planetary Science Letters*, *217*.
701 Manighetti, I., Campillo, M., Bouley, S., & Cotton, F. (2007). Earthquake scaling, fault
702 segmentation, and structural maturity. *Earth and Planetary Science Letters*,
703 *253*(3–4), 429–438. https://doi.org/10.1016/j.epsl.2006.11.004
704 Manighetti, I., Mercier, A., & De Barros, L. (2021). Fault Trace Corrugation and
705 Segmentation as a Measure of Fault Structural Maturity. *Geophysical Research*
706 *Letters*, *48*(20), e2021GL095372. https://doi.org/10.1029/2021GL095372

Mansfield, C., & Cartwright, J. (2001). Fault growth by linkage: observations and implications from analogue models. *Journal of Structural Geology*, *23*(5), 745–763. https://doi.org/10.1016/S0191-8141(00)00134-6

Manzocchi, T., Walsh, J. J., & Nicol, A. (2006). Displacement accumulation from earthquakes on isolated normal faults. *Journal of Structural Geology*, *28*(9), 1685–1693. https://doi.org/10.1016/j.jsg.2006.06.006

McLeod, A. E., Dawers, N. H., & Underhill, J. R. (2000). The propagation and linkage of normal faults: insights from the Strathspey–Brent–Statfjord fault array, northern North Sea. *Basin Research*, *12*, 263–284.

Mildon, Z. K. (2017). *The link between earthquakes and structural geology; the role of elapsed time, 3D geometry and stress transfer in the central Apennines, Italy*. University College London.

Mildon, Z. K., Roberts, G. P., Faure Walker, J. P., Wedmore, L., & McCaffrey, K. J. W. (2016). Active normal faulting during the 1997 seismic sequence in Colfiorito, Umbria: Did slip propagate to the surface? *Journal of Structural Geology*. https://doi.org/10.1016/j.jsg.2016.08.011

Mildon, Z. K., Roberts, G. P., Faure Walker, J. P., & Iezzi, F. (2017). Coulomb stress transfer and fault interaction over millennia on non-planar active normal faults: the Mw 6.5-5.0 seismic sequence of 2016-2017, central Italy. *Geophysical Journal International*, *210*(2), 1206–1218. https://doi.org/10.1093/gji/ggx213

Mildon, Z. K., Roberts, G. P., Faure Walker, J. P., & Toda, S. (2019). Coulomb pre-stress and fault bends are ignored yet vital factors for earthquake triggering and hazard. *Nature Communications*, *10*(1). https://doi.org/10.1038/s41467-019-10520-6

730 Nicol, A., Walsh, J., Berryman, K., & Nodder, S. (2005). Growth of a normal fault by the
731 accumulation of slip over millions of years. *Journal of Structural Geology*, *27*,
732 327–342. https://doi.org/10.1016/j.jsg.2004.09.002
733 Nixon, C. W., Vaagan, S., Sanderson, D. J., & Gawthorpe, R. L. (2019). Spatial
734 distribution of damage and strain within a normal fault relay at Kilve, U.K. *Journal*
735 *of Structural Geology*, *118*, 194–209. https://doi.org/10.1016/j.jsg.2018.10.016
736 Okubo, K., Bhat, H. S., Rougier, E., Marty, S., Schubnel, A., Lei, Z., et al. (2019).
737 Dynamics, Radiation, and Overall Energy Budget of Earthquake Rupture With
738 Coseismic Off-Fault Damage. *Journal of Geophysical Research: Solid Earth*,
739 *124*(11), 11771–11801. https://doi.org/10.1029/2019JB017304
740 Pace, B., Bocchini, G. M., & Boncio, P. (2014). Do static stress changes of a moderate-
741 magnitude earthquake significantly modify the regional seismic hazard? Hints
742 from the L'Aquila 2009 normal-faulting earthquake (Mw 6.3, central Italy). *Terra*
743 *Nova*, *26*(6), 430–439. https://doi.org/10.1111/ter.12117
744 Perrin, C., Manighetti, I., Ampuero, J.-P., Cappa, F., & Gaudemer, Y. (2016). Location of
745 largest earthquake slip and fast rupture controlled by along-strike change in fault
746 structural maturity due to fault growth. *Journal of Geophysical Research: Solid*
747 *Earth*, *121*(5), 3666–3685. https://doi.org/10.1002/2015JB012671
748 Piccardi, L., Gaudemer, Y., Tapponnier, P., & Boccaletti, M. (1999). Active oblique
749 extension in the central Apennines (Italy): evidence from the Fucino region.
750 *Geophysical Journal International*, *139*(2), 499–530.
751 https://doi.org/10.1046/j.1365-246x.1999.00955.x
752 Pizzi, A., Di Domenica, A., Gallovič, F., Luzi, L., & Puglia, R. (2017). Fault Segmentation
753 as Constraint to the Occurrence of the Main Shocks of the 2016 Central Italy

754 Seismic Sequence. *Tectonics*, *36*(11), 2370–2387.
755 https://doi.org/10.1002/2017TC004652
756 Roberts, G. P. (2007). Fault orientation variations along the strike of active normal fault
757 systems in Italy and Greece: Implications for predicting the orientations of
758 subseismic-resolution faults in hydrocarbon reservoirs. *AAPG Bulletin*, *91*(1), 1–
759 20. https://doi.org/10.1306/08300605146
760 Roberts, G. P., & Michetti, A. M. (2004). Spatial and temporal variations in growth rates
761 along active normal fault systems: an example from The Lazio–Abruzzo
762 Apennines, central Italy. *Journal of Structural Geology*, *26*(2), 339–376.
763 https://doi.org/10.1016/S0191-8141(03)00103-2
764 Roberts, G. P., Iezzi, F., Sgambato, C., Robertson, J., Beck, J., Mildon, Z. K., et al. (2025).
765 Characteristics and modelling of slip-rate variability and temporal earthquake
766 clustering across a distributed network of active normal faults constrained by in
767 situ 36Cl cosmogenic dating of fault scarp exhumation, central Italy. *Journal of*
768 *Structural Geology*, *195*, 105391. https://doi.org/10.1016/j.jsg.2025.105391
769 Roche, V., Camanni, G., Childs, C., Manzocchi, T., Walsh, J., Conneally, J., et al. (2021).
770 Variability in the three-dimensional geometry of segmented normal fault
771 surfaces. *Earth-Science Reviews*, *216*, 103523.
772 https://doi.org/10.1016/j.earscirev.2021.103523
773 Rodriguez Piceda, C., Mildon, Z. K., Andrews, B. J., Visini, F., Ampuero, J. P., & Ende, M.
774 van den. (2025). Spatially heterogenous Holocene slip rates drive seismic
775 sequence variability on normal faults. *Seismica*, *4*(2).
776 https://doi.org/10.26443/seismica.v4i2.1682

777 Sagy, A., Brodsky, E. E., & Axen, G. J. (2007). Evolution of fault-surface roughness with
778 slip. *Geology*, *35*(3), 283–286. https://doi.org/10.1130/G23235A.1
779 Schirripa Spagnolo, G., Mercuri, M., Billi, A., Carminati, E., & Galli, P. (2021). The
780 Segmented Campo Felice Normal Faults: Seismic Potential Appraisal by
781 Application of Empirical Relationships Between Rupture Length and Earthquake
782 Magnitude in the Central Apennines, Italy. *Tectonics*, *40*(7), e2020TC006465.
783 https://doi.org/10.1029/2020TC006465
784 Servizio Geologico d'Italia. (2009a). Geological sheet 369 "Sulmona" (scale 1:50,000).
785 Retrieved from https://www.isprambiente.gov.it/Media/carg/abruzzo.html
786 Servizio Geologico d'Italia. (2009b). Geological Sheet n. 359 "L'Aquila" (scale 1:50,000).
787 Retrieved from https://www.isprambiente.gov.it/Media/carg/abruzzo.html
788 Servizio Geologico d'Italia. (2009c). Geological Sheet n.360 "Torre de Passeri" (scale
789 1:50,000). Retrieved from
790 https://www.isprambiente.gov.it/Media/carg/abruzzo.html
791 Servizio Geologico d'Italia. (2009d). Geological Sheet n.368 "Avezzano" (scale
792 1:50,000). Retrieved from
793 https://www.isprambiente.gov.it/Media/carg/abruzzo.html
794 Sgambato, C., Faure Walker, J. P., & Roberts, G. P. (2020). Uncertainty in strain-rate from
795 field measurements of the geometry, rates and kinematics of active normal
796 faults: Implications for seismic hazard assessment. *Journal of Structural*
797 *Geology*, *131*, 103934. https://doi.org/10.1016/j.jsg.2019.103934
798 Shipton, Z. K., Evans, J. P., Abercrombie, R. E., & Brodsky, E. E. (2006). The missing sinks:
799 Slip localization in faults, damage zones, and the seismic energy budget. In R.
800 Abercrombie, A. McGarr, H. Kanamori, & G. Di Toro (Eds.), *Geophysical*

Monograph Series (Vol. 170, pp. 217–222). Washington, D. C.: American Geophysical Union. https://doi.org/10.1029/170GM22

Steacy, S. J., & McCloskey, J. (1998). What controls an earthquake's size? Results from a heterogeneous cellular automaton. *Geophysical Journal International*, *133*(1), F11–F14. https://doi.org/10.1046/j.1365-246X.1998.1331548.x

Stirling, M., Goded, T., Berryman, K., & Litchfield, N. (2013). Selection of earthquake scaling relationships for seismic-hazard analysis. *Bulletin of the Seismological Society of America*, *103*(6), 2993–3011. https://doi.org/10.1785/0120130052

Tarquini, S., Vinci, S., Favalli, M., Doumaz, F., Fornaciai, A., & Nannipieri, L. (2012). Release of a 10-m-resolution DEM for the Italian territory: Comparison with global-coverage DEMs and anaglyph-mode exploration via the web. *Computers & Geosciences*, *38*(1), 168–170. https://doi.org/10.1016/j.cageo.2011.04.018

Tesson, J., Benedetti, L., Godard, V., Novaes, C., Fleury, J., & the ASTER Team. (2021). Slip rate determined from cosmogenic nuclides on normal-fault facets. *Geology*, *49*(1), 66–70. https://doi.org/10.1130/G47644.1

Testa, A., Boncio, P., Di Donato, M., Mataloni, G., Brozzetti, F., & Cirillo, D. (2019). Mapping the geology of the 2016 Central Italy earthquake fault (Mt. Vettore – Mt. Bove fault, Sibillini Mts.): geological details on the Cupi – Ussita and Mt. Bove – Mt. Porche segments and overall pattern of coseismic surface faulting. https://doi.org/10.3301/GFT.2019.03

Thakur, P., & Huang, Y. (2021). Influence of Fault Zone Maturity on Fully Dynamic Earthquake Cycles. *Geophysical Research Letters*, *48*(17), e2021GL094679. https://doi.org/10.1029/2021GL094679

824 Thingbaijam, K. K. S., Martin Mai, P., & Goda, K. (2017). New Empirical Earthquake
825 Source-Scaling Laws. *Bulletin of the Seismological Society of America*, *107*(5),
826 2225–2246. https://doi.org/10.1785/0120170017
827 Tucker, G. E., McCoy, S. W., Whittaker, A. C., Roberts, G. P., Lancaster, S. T., & Phillips, R.
828 J. (2011). Geomorphic significance of postglacial bedrock scarps on normal-fault
829 footwalls. *Journal of Geophysical Research: Earth Surface*, *116*(F1).
830 https://doi.org/10.1029/2010JF001861
831 Walsh, J. J., Nicol, A., & Childs, C. (2002). An alternative model for the growth of faults.
832 *Journal of Structural Geology*, *24*(11), 1669–1675. https://doi.org/10.1016/S0191-
833 8141(01)00165-1
834 Walsh, J. J., Bailey, W. R., Childs, C., Nicol, A., & Bonson, C. G. (2003). Formation of
835 segmented normal faults: A 3-D perspective. *Journal of Structural Geology*,
836 *25*(8), 1251–1262. https://doi.org/10.1016/S0191-8141(02)00161-X
837 Walters, R. J., Elliott, J. R., D'Agostino, N., England, P. C., Hunstad, I., Jackson, J. A., et al.
838 (2009). The 2009 L'Aquila earthquake (central Italy): A source mechanism and
839 implications for seismic hazard. *Geophysical Research Letters*, *36*(17), 2–7.
840 https://doi.org/10.1029/2009GL039337
841 Wells, D. L., & Coppersmith, K. J. (1994). New Empirical Relationships among
842 Magnitude, Rupture Length, Rupture Width, Rupture Area, and Surface
843 Displacement. *Bulletin of the Seismological Society of America*, *84*(4), 974–
844 1002.
845 Wilkinson, M. W., Roberts, G. P., McCaffrey, K. J. W., Cowie, P. A., Faure Walker, J. P.,
846 Papanikolaou, I. D., et al. (2015). Slip distributions on active normal faults
847 measured from LiDAR and field mapping of geomorphic offsets: an example

from L'Aquila, Italy, and implications for modelling seismic moment release. *Geomorphology*, *237*, 130–141. https://doi.org/10.1016/j.geomorph.2014.04.026